GEOPHYSICS, VOL. 77, NO. 5 (SEPTEMBER-OCTOBER 2012); P. WC133–WC147, 17 FIGS., 2 TABLES.
10.1190/GEO2012-0135.1

# 3D edge detection seismic attributes used to map potential conduits for water and methane in deep gold mines in the Witwatersrand basin, South Africa

Musa S. D. Manzi[1], Raymond J. Durrheim[2], Kim A. A. Hein[1], and Nick King[3]

## ABSTRACT

Inrushes of ground water and the ignition of flammable gases pose risks to workers in deep South African gold mines. Large volumes of water may be stored in solution cavities in dolomitic rocks that overlie the Black Reef (BLR) Formation, while there are several possible sources for methane, namely, coal seams, kerogen found in some gold ore bodies, or methane introduced by igneous intrusions. Potential conduits that may transport water and methane to underground workings were mapped using 3D reflection seismic data. Edge detection attributes successfully identified many faults, some with displacements as small as 10 m. Faults that displace the Ventersdorp Contact Reef (VCR) and the BLR horizons were of special interest, as known occurrences of fissure water and methane in underground workings show a good correlation with faults that were imaged on the VCR and BLR horizons. Because there are uncertainties in determining the linkage of faults with aquifers and methane sources, it is considered prudent to assume that all structures that displace the VCR and BLR horizons are potential conduits.

## INTRODUCTION

The deep gold mines of South Africa employ labor-intensive mining methods with as many as 5000 miners working in a single shaft. The miners face various hazards, including rock falls, rockbursts associated with mining-induced seismic events, moving trains transporting ore and waste rock, handling of explosives, inrushes of water, and flammable gases (Adams et al., 2007). In this paper, we discuss the use of 3D seismics to address the risks posed by flooding and flammable gases. Mining engineers have devised many ways to minimize the risks associated with water inrush and methane ignition. However, the mechanism whereby methane and water is transported to mine workings is not well understood.

The 3D seismic reflection technique was first implemented to image oil and gas reservoirs in the 1960s (Pretorius et al., 1994; Salisbury et al., 2003). Over the past 20 years, 3D seismics has been used worldwide for mine planning, design, and risk reduction in the deep metal mines (Milkereit et al., 1996, 2000; Pretorius et al., 2000; Trickett et al., 2004; Malehmir and Bellefleur, 2009; Malehmir et al., 2012). Recently, the technique has played an increasingly important role in the exploration of the Witwatersrand basin in South Africa, being used to delineate major gold-bearing horizons for mine planning and production purposes (Pretorius et al., 2003; Salisbury et al., 2003; Stevenson et al., 2003; Manzi et al., 2012). Although 3D seismic surveys are expensive relative to linear 2D surveys, they give full representations of the subsurface. Therefore, 3D seismic surveys offer great advantage for processing and interpretation of the seismic data.

Since the late 1980s, global developments in the acquisition, processing, and interpretation of 3D seismic data have made the technique increasingly effective to the point that it has become fundamental and a well-established method in the development of the seismic and structural models.

In this study, we use high-resolution 3D seismic data acquired in the West Rand and West Wits Line (Carletonville) gold fields (Figure 1) to investigate the role that faults might play in transporting water and methane to mine workings. To achieve this goal, we use 3D horizon-related edge detection attribute analysis to better define fault architectures that often are difficult to resolve in

Manuscript received by the Editor 18 April 2012; published online 6 September 2012.
[1]University of the Witwatersrand, School of Geosciences, Johannesburg, Republic of South Africa. E-mail: Musa.Manzi@students.wits.ac.za; kim.ncube-hein@wits.ac.za.
[2]University of the Witwatersrand, School of Geosciences, Johannesburg, Republic of South Africa; and CSIR Centre for Mining Innovation, Johannesburg, Republic of South Africa. E-mail: Raymond.Durrheim@wits.ac.za; RDurrhei@csir.co.za.
[3]South Deep Gold Mine, Gold Fields Limited, Johannesburg, Republic of South Africa. E-mail: nick.king@goldfields.co.za.

seismic sections. Horizon attributes, such as dip and dip azimuth, were introduced by Dalley et al. (1989) and Rijks and Jauffred (1991).

Recent improvements in mapping techniques implemented in the interpretation software, such as edge detection attributes, has allowed optimum imaging of subtle faults (throw less than ~15 m). This study is, to our knowledge, the first to use edge detection seismic attributes to study the relationships between faults and sources of water and methane in the Witwatersrand basin. The application of these techniques has led to a robust definition of subtle faults that has direct impact on mine planning decisions.

## RISKS POSED BY FLOODING AND FLAMMABLE GASES

In the West Rand and West Wits Line gold fields of the Witwatersrand basin, gold-bearing strata are overlain by the Malmani Dolomite sequence that measures up to a kilometer in thickness (Figure 2a and 2b). The dolomite potentially is charged with large volumes of groundwater in fissures and solution cavities. The sequence is intruded by vertical dikes that are impervious to water and divide the aquifer into several compartments. To mitigate the risk of water inrushes when sinking a shaft or developing a tunnel, test boreholes are drilled into the surrounding rock mass. If any water is encountered, the holes are sealed.

The control of water is more difficult during stoping operations as the hangingwall may sag with development of fractures that cannot be easily sealed.

Until 1968, the flow of water into the stopes at many mines was accepted as inevitable. Water emerging from fissures was channeled into drains, pumped to the surface, and transported away from the mine area by means of canals. On 26 October 1968, a massive inrush of water occurred at No. 4 Shaft of West Driefontein mine, overwhelming the capacity of the pumps (Cousens and Garrett, 1969). The flow continued for 23 days before it was stemmed. All 1400 miners in the area of No. 4 shaft were safely evacuated, but production at the mine, at that time the world's biggest gold producer, was severely affected.

Following the West Driefontein disaster, a new strategy was implemented to mitigate the risk of water inrushes from overlying dolomite compartments. The compartments were dewatered by sustained pumping, and the water disposed of in such a way that it could not find its way back into an aquifer (Ngcobo, 2006). Although the dewatering strategy certainly was effective, it triggered sinkholes and was costly to sustain. Much of the ore in Witwatersrand gold mines has been extracted, and production in many mines has decreased or ceased. Consequently, the pumping of ground water has slowed or stopped. The water level is rising in some compartments, raising concerns about the integrity of water-barrier pillars that protect adjacent operating mines.

Furthermore, many of the gold mines are classified as "fiery" as they are prone to the influx of flammable gases, principally methane. The ignition of these gases have led to several disasters, including at Mponeng mine in the West Wits Line gold field on 29 July 1999, causing 19 deaths and two injuries (Motaung, 2000), and at Beatrix mine in the Free State gold field on 15 May 2000 and 8 May 2001, causing seven and 13 deaths, respectively (Kritzinger, 2001). Also, on 11 November 1999, a 16-m-long cavity was formed following a normal development blast at a depth of 2800 m in the Moab Khutsong mine in the Klerksdorp gold field (Ortlepp, 2001).

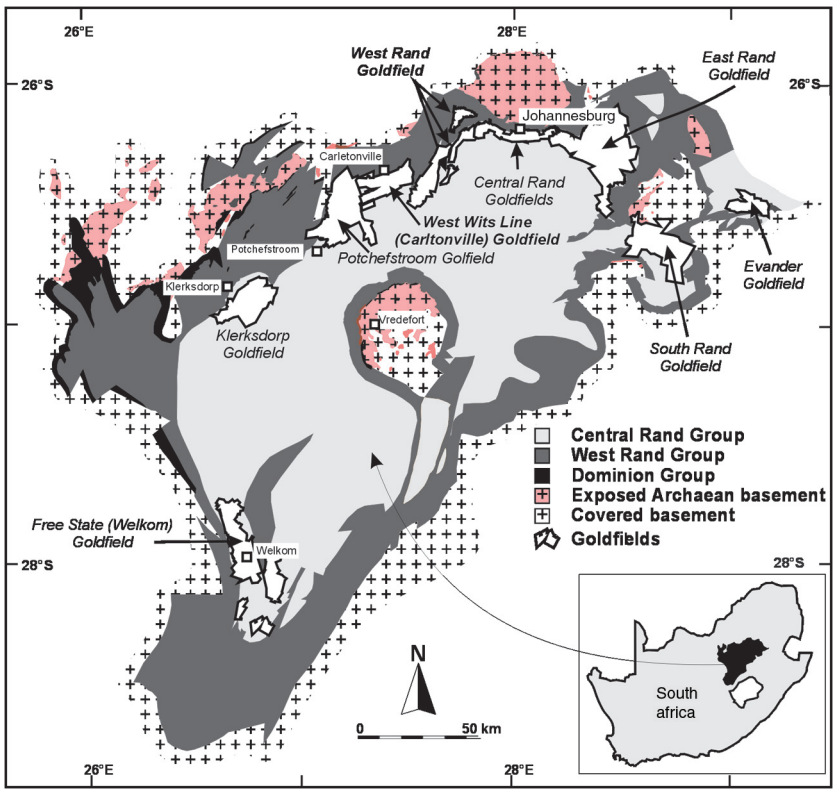


Figure 1. The location map of the West Rand and West Wits Line (Carletonville) gold fields of the Witwatersrand basin in South Africa (after Dankert and Hein, 2010).

It was interpreted to be the result of an outburst of highly compressed gas. Fortunately, no ignition occurred, although sampling of the return air from the tunnel showed a high concentration of flammable gas, and a strong smell of sulphurated hydrogen was detected.

The origin and transportation of the combustible gases found in the Archean quartzite and conglomerate units of the Witwatersrand basin has been investigated by several workers and reviewed by Cook (1998). Possible sources include primordial methane transported from the mantle by granitic intrusions and syenite dikes; kerogen, interpreted to be derived from ancient algal mats that are sometimes found together with gold, notably in an ore body known as the Carbon Leader Reef; or coal seams found in much younger Karoo strata. The Karoo Supergroup overlies much of the Witwatersrand basin, and its coal seams are regarded as the main source of methane into the Witwatersrand basin gold mines, especially in the Free State gold field (Spencer and Walter, 2000).

The methane migrates from the source to mine workings through faults and fractures, either as a gas or dissolved in ground water. The pressure decreases when a void is reached and the gas exsolves into the atmosphere. Permeability is confined to joints and faults as the host rocks are not porous. Major faults can provide conduits for water ingress because the roughness of the fault walls permits the presence of a network of small cavities that can be water-bearing (Bekker, 1986). Many dikes have major fault planes at their contact margins that can act as conduits.

## GEOLOGIC SETTING

The gold-bearing conglomerates (or reefs) of the Archean Witwatersrand Supergroup, which crop out near present day Johannesburg, were discovered in 1886. The West Rand and West Wits Line goldfields, located on the northern rim of the Witwatersrand basin about 40 and 60 km southwest of Johannesburg, are concealed by younger overlying strata. The gold fields were discovered in the

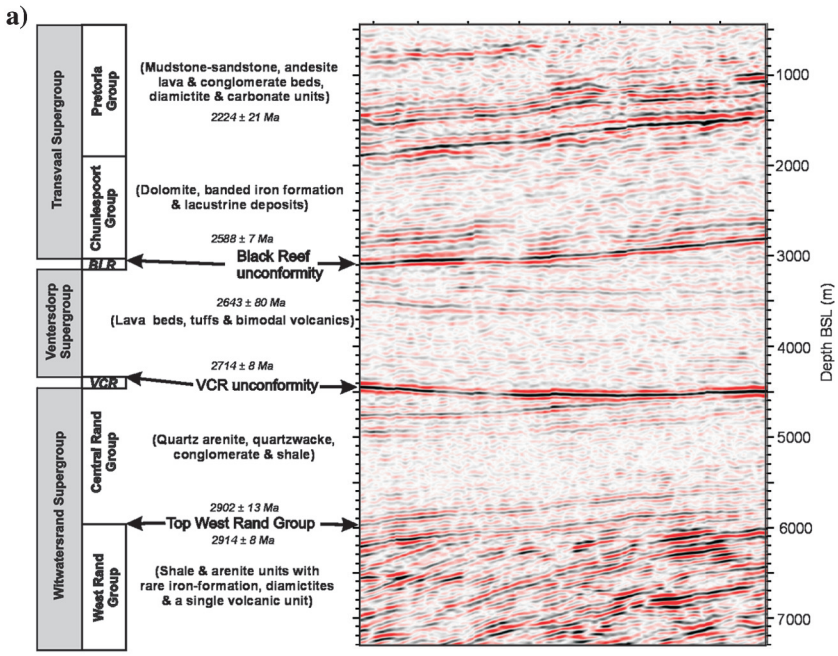


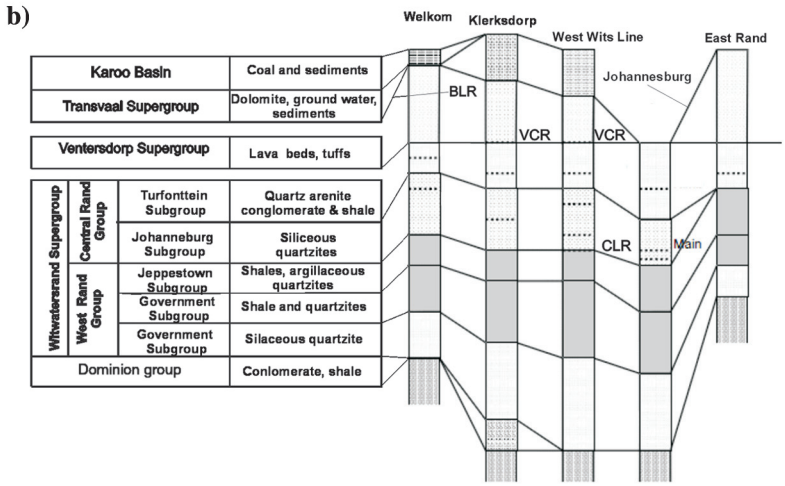


Figure 2. (a) Generalized stratigraphy of the West Wits Line gold field, derived from depth converted prestack time migrated (PSTM) seismic section. Geochronological data and geology provided by Dankert and Hein (2010). (b) Generalized stratigraphic column of the Witwatersrand basin showing important gold-bearing horizons or reefs within the Central Rand Group. The West Wits Line and West Rand gold fields are overlain by the dolomitic aquifers of the Transvaal Supergroup. Karoo sediments and coals have been eroded in these gold fields (Cook, 1998).

1930s through drilling that was guided by magnetic and gravity surveys. The geology and structural setting of the Witwatersrand basin is documented by many authors, including Coward et al. (1995), Gibson et al. (2000), Jolley et al. (2004), Beach and Smith (2007), and Dankert and Hein (2010). In summary, the Witwatersrand Supergroup unconformably overlies the Dominion Group. The Supergroup is subdivided into the (lower) West Rand and (upper) Central Rand groups (McCarthy, 2006; Dankert and Hein, 2010) (Figure 2a and 2b). Unconformably overlying the Central Rand Group is the Ventersdorp Supergroup, with the Ventersdorp Contact Reef (VCR) of the Venterspost Formation. The Ventersdorp Supergroup consists of the volcanic Klipriviersberg Group, the predominantly metasedimentary Platberg Group, and the Pniel Group (Coward et al., 1995; Jolley et al., 2004). Unconformably overlying the Ventersdorp Supergroup is the relatively thin Black Reef Formation (BLR), which is the basal lithostratigraphic unit of the Transvaal Supergroup. This Supergroup is divided into the Chuniespoort Group and the Pretoria Group. Considerable volumes of groundwater are stored within the dolomitic aquifers of the Malmani Subgroup of the Chuniespoort Group (McCarthy, 2006; Mambane et al., 2011) (Figure 2a and 2b).

This study focuses on Driefontein, Kloof and South Deep gold mines (owned by Gold Fields Ltd.) and Mponeng, Tautona, and Savuka gold mines (owned by AngloGold Ashanti), and their down-dip extensions (Figure 3a). The southern portion of the Kloof mining areaformerly was known as the Leeudoorn mine (Figure 3a). The down-dip extension of Mponeng, Savuka, Tautona, and Driefontein was known as Western Ultra Deep Levels (WUDLs).

The West Wits Line and West Rand goldfields are separated by the Bank Fault (Figure 3a). The Driefontein mine is situated west of the Bank Fault, and is one of the largest mines in the West Wits Line goldfield. The most important ore body at Driefontein mine is the Carbon Leader Reef, which constitutes about 75% of the ore reserve, with the VCR providing about 20%. The Kloof mine lies to the east of the Bank Fault (Figure 3a); three reefs are exploited,

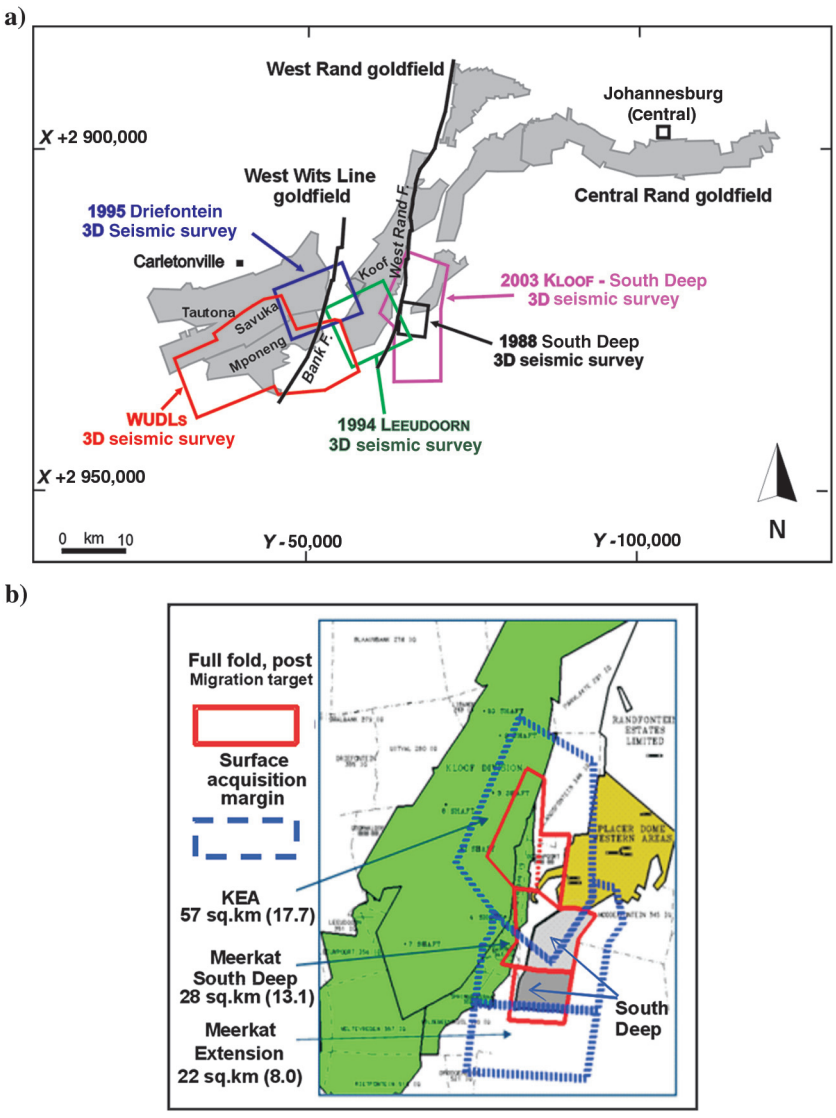


Figure 3. (a) The location of historical surveys for Kloof, South Deep, Driefontein, and WUDLs (after Manzi et al., 2012). (b) KEA and Meerkat (South Deep) seismic survey acquisition margin and targeted areas.

although the VCR is by far the largest contributor, representing 88% of the ore reserve. The South Deep mine is situated to the east of Kloof mine and the West Rand Fault (Figure 3a and 3b). With some 78.2 million ounces of resources and 29.3 million ounces of reserves, South Deep is the largest undeveloped gold ore body in the world. The bulk of the ore is found in the Upper Elsburg Reefs, although some VCR also is present.

Two prominent seismic reflectors were used to map the geologic structure in this study, namely the bottom contact of the BLR which lies at the base of the Transvaal Supergroup, and the bottom contact of the Ventersdorp Supergroup lavas, which marks the position of the VCR ore body.

## DESIGN, ACQUISITION, AND PROCESSING OF THE 3D SEISMIC SURVEY

The seismic data covering the extensions of the Kloof and South Deep mines were acquired in 2003. The primary goal of the seismic survey was to image the VCR ore body. Stratigraphic dips of 15°–35° were anticipated west of the West Rand Fault and 10°–20° to the east of the West Rand Fault. The VCR consists of conglomerates with varying clast sizes in a quartzite matrix. The VCR rarely exceeds 1.5 m in thickness and is too thin to be directly detected by surface reflection seismics. Instead, it is the boundary between the lavas of the overlying Ventersdorp Supergroup and the quartzite units of the Central Rand Group that is imaged because the quartzite units have a lower density and seismic velocity. A secondary goal was to image the base of the BLR, which lies some 1500 m above the VCR at depths of 200–1500 m. The BLR Formation is a thin quartzite separating the Ventersdorp lavas below from the dolomites of the Chuniespoort Group. The dolomites have higher density and seismic velocity; therefore, it is the Ventersdorp-Chuniespoort contact that gives rise to a strong seismic reflection.

The survey consisted of 4155 shot points recorded over an area of approximately 96 $km^2$ covering the Kloof Extension Area (KEA), Meerkat (South Deep Mine), and Meerkat Extension areas (Figure 3b). The acquisition parameters are summarized in Table 1. To avoid any reduction in data quality owing to poor source and receiver coupling, scattering of energy, attenuation of high frequencies, or potentially poor static solutions, no shots or receivers were located on rock dumps and slimes dams located on the Kloof and South Deep mines. The placement of compensation shots was monitored carefully to ensure that the fold of coverage was maintained and that the minimum offsets within each bin remained acceptable. The compensation shot strategy only was feasible because the target depth is in excess of about 3000 m beneath the obstacles. Although a detailed description of the survey design is beyond the scope of this paper, the following points merit mention as they are relevant to the resolution of the survey.

- A $25 \times 25$ $m^2$ bin size was chosen to avoid spatial aliasing up to a stratigraphic dip of 35° (the maximum dip observed at Kloof mine), based on interval velocity of 6500 m/s and a maximum frequency of 100 Hz (the upper limit of the sweep used in the survey).
- A maximum shot-receiver offset of 3325 m was chosen to provide fullfold coverage over the range of VCR target depths between 3000 and 4200 m. A greater maximum offset would run the risk of producing data recorded at less than full fold at the shallower target range.
- The nominal fold of coverage was 36 to the west of the West Rand Fault, and 30 to the east of the fault. This represents a significant increase in fold compared with all previous deep Witwatersrand basin 3D seismic surveys, which were

**Table 1. Field acquisition parameters for 2003 3D Kloof-South Deep seismic surveys.**

| Recorded by | CGG | Crew 303,32,44 |
|---|---|---|
| Instrumentation | System | Sercel 408 |
| | Geophones | 10 Hz |
| | Data media | 3490 Cartridge |
| | Data format | SEGD IEEE Demultiplexed |
| | Record length | 6 s |
| | Sample interval | 2 ms |
| | System polarity | SEG standard |
| Parameters | Bin dimensions | $25 \times 25$ m |
| | Survey pattern | Orthogonal |
| | Live patch asymmetrical | 12 lines × 108 1296 channels |
| | Live patch symmetrical | 12 lines × 90 1080 channels |
| | Asymmetrical split | 1–45 ∗ 46–108 Ch 108 to the east |
| | Symmetrical split | 1–45 ∗ 46–90 |
| | Shot line separation | 450 m |
| | Shot line direction | 9.51° |
| | Shot line angle to receiver line | 90° |
| | Shot point separation | 50 m |
| | Total number of shot points | 4155 |
| | Receiver line separation | 400 m |
| | Receiver line direction | 99.51° |
| | Receiver point separation | 50 m |
| | Total number of receiver points | 4957 |
| | Array | Linear, 12 phones/string |
| | Array length | Variable 36–85 m — bunched, length based on topography |
| Source | Vibroseis | |
| | Pattern | 4 Vibs inline 45-m array |
| | Sweep | 16 s 12–96 Hz |
| | | 4 sweeps/$V_P$ |

**Table 2. Processing parameters for 2003 3D Kloof-South Deep and 1994 Leeudoorn seismic data sets.**

| Processing route | Parameters |
|---|---|
| Data reformat | From SEGD to Promax internal format |
| Trace editing | Air-blast attenuation applied |
| Geometry application | Source, receiver, offsets, etc., assigned to each trace |
| Gain recovery: spherical divergence correction | $1/(TV \wedge 2)$, where V = 5500 m/s |
| Surface consistent spiking deconvolution | Operator design window at 0 m offset: 100–2500 ms, operator length: 120 ms, white noise stabilization: 1% |
| Zero-phase spectral whitening | Eight frequency windows, 500-ms sliding window |
| 3D refraction statics correction | Surface layer V0 = 1200 m/s (constant), seismic datum elevation: 1500 m a.m.s.l |
| Statics application | Smooth processing datum |
| First-pass interactive velocity analysis | Every 600 m in crossline and inline directions |
| First-pass surface consistent residual statics | Maximum power autostatics, 300-ms time gate around flattened horizons |
| Interim stack: Leeudoorn and Kloof-South Deep | Data sets stacked separately, 35% stretch mute and 500-ms AGC applied |
| Prestack phase rotation and time-shift to match Leeudoorn and Kloof data sets | Leeudoorn data: time shift of −8 ms and 90° phase shift |
| Prestack merge of Kloof-South Deep and Leeudoorn data sets | Refraction statics calculated on the merged data and tied to upholes |
| Second-pass interactive velocity analysis | Every 600 m in crossline and inline directions |
| Second-pass surface consistent residual statics application | Maximum power autostatics, 300-ms time gate around flattened horizons |
| CDP trim statics | Nonsurface consistent CDP statics |
| DMO velocity analysis | Full 3D Kirchoff DMO using 50-m inline and crossline distance |
| Prestack time migration (PSTM) flow | |
| First-pass PSTM velocity analysis | DMO velocities removed and PSTM velocities picked |
| PSTM | Full 3D Kirchoff using velocity model from smoothed first pass PSTM velocities |
| Second-pass PSTM velocity analysis | Second pass PSTM velocities picked |
| NMO correction | Second pass PSTM velocities applied |
| Stack | |
| Band-pass frequency filter | Time varient Ormsby zero-phase filter, 0–1400 ms: 15/20 – 80/90 Hz |
| Depth conversion | Using interval velocities derived from borehole data and BLR and VCR time horizons |
| WUDLS data merge | Kloof-South Deep data depth shifted to 1830 m a.m.s.l datum and regridded to match WUDLs orientation |

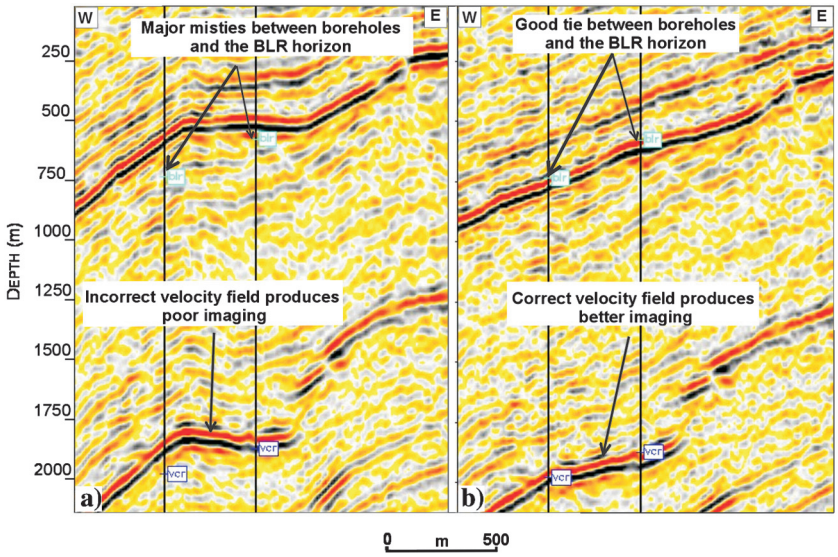


Figure 4. Depth converted time migrated sections using finite difference migration algorithm. (a) Unsmoothed velocity field provides a very stretched seismic horizons and distorted structures (possibly undermigrations). This shows a huge depth mis-tie between the VCR and BLR horizons and borehole control. (b) Smoothed velocity field provides stable seismic horizons and structures. These results show a very good depth tie between the VCR and BLR horizons and boreholes.

typically 20 fold. This fold was recorded with no increase in costs relative to earlier surveys due to the ability of the instrumentation to deal with larger numbers of receivers.

- The migration aperture varied depending on target depth and dip. The dip migration aperture (margin) was designed so that it could provide fullfold coverage of the subsurface target area after migration. The diffraction migration aperture of 1125 m (at 4200 m VCR target depth with 15° dip) was chosen to provide 75% of diffraction energy at all predicted major fault cutoffs of the VCR.

The processing parameters for Kloof, South Deep, and Leeudoorn data sets are summarized in Table 2. The table does not list the DMO to depth migration (finite-difference poststack method) tests initially applied to the data sets. The more detailed data processing and merging steps undertaken are described in Manzi et al. (2012). The following summary highlights important processing steps that are relevant to this paper, mainly velocity analysis. The 2003 Kloof-South Deep prestack data were merged with the reprocessed 1994 Leeudoorn data that covers the southern portion of Kloof mine (Figure 3a and 3b). The Leeudoorn survey consisted of 5739 shots recorded over an area of 70 km$^2$. The 1994 Leeudoorn and 2003 Kloof-South Deep data sets were processed individually through to residual statics to allow comparison of the two data sets. Appropriate static and phase corrections were calculated and applied before prestack merging of the two data sets (Table 2). The merged data set covers an area of 147 km$^2$ with 9894 shot points.

Prestack processing included radial filtering to remove ground roll, Wiener-Levinson deconvolution and zero-phase spectral

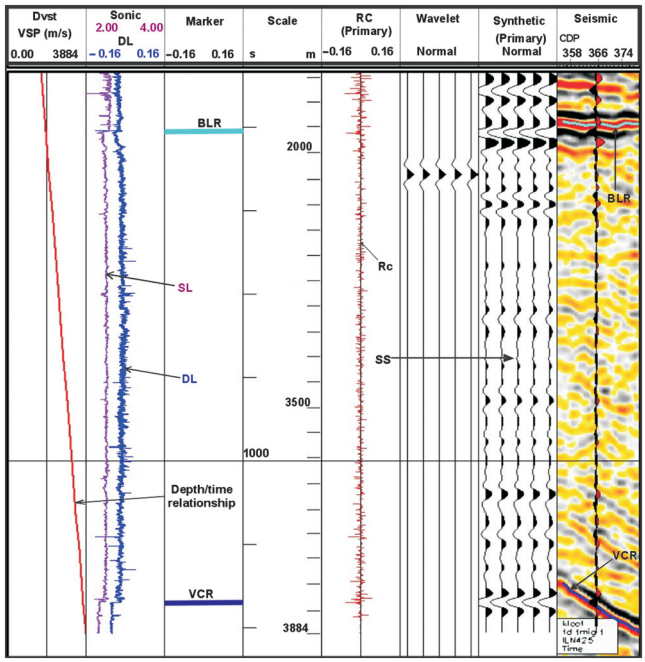


Figure 5. Seismic data and the synthetic seismogram derived from sonic and density log for the borehole, showing a good correlation with the BLR and VCR horizons. DL: Density log; Rc: Reflection coefficients; SL: Sonic log; SS: Synthetic seismogram; BLR: Black Reef; VCR: Ventersdorp Contact Reef.

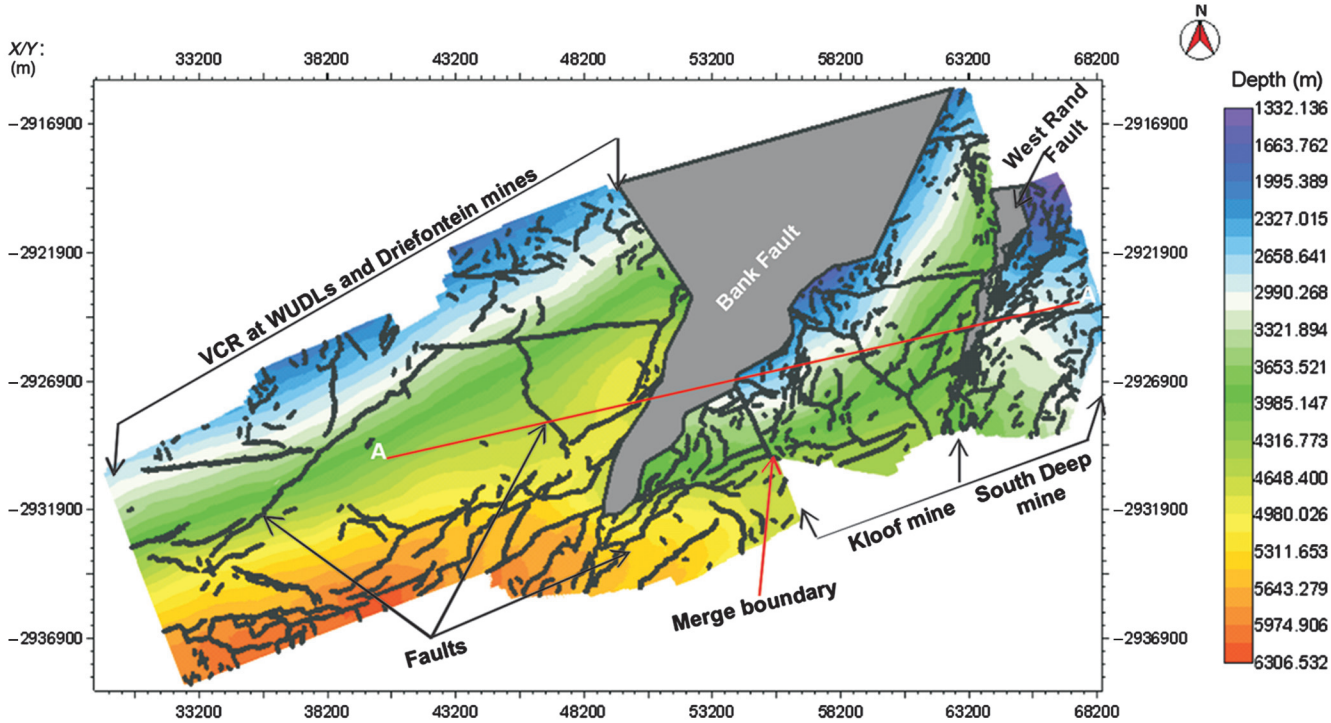


Figure 6. Detailed depth structure map of the Venterdorp Contact Reef (VCR) derived from conventional picking across survey areas, showing faults of all strikes and dips.

whitening to improve resolution, the application of residual statics and velocity analysis. Time migration was performed using the finite difference algorithm. The BLR and VCR time horizons were picked, using borehole logs for control. A three-layer interval velocity model was derived. The layers are:

- datum to BLR (yielding the interval velocity for the Transvaal Supergroup rocks)
- BLR to VCR (interval velocity of Klipriviersberg lavas)
- below VCR to Booysens Shale (using stacking velocity due to no borehole control)

The velocity field used for the 3D finite-difference partial prestack time migration (PSTM) and for depth conversion had short wavelength velocity variations due to irregular borehole spacing and very densely spaced underground boreholes. This resulted in

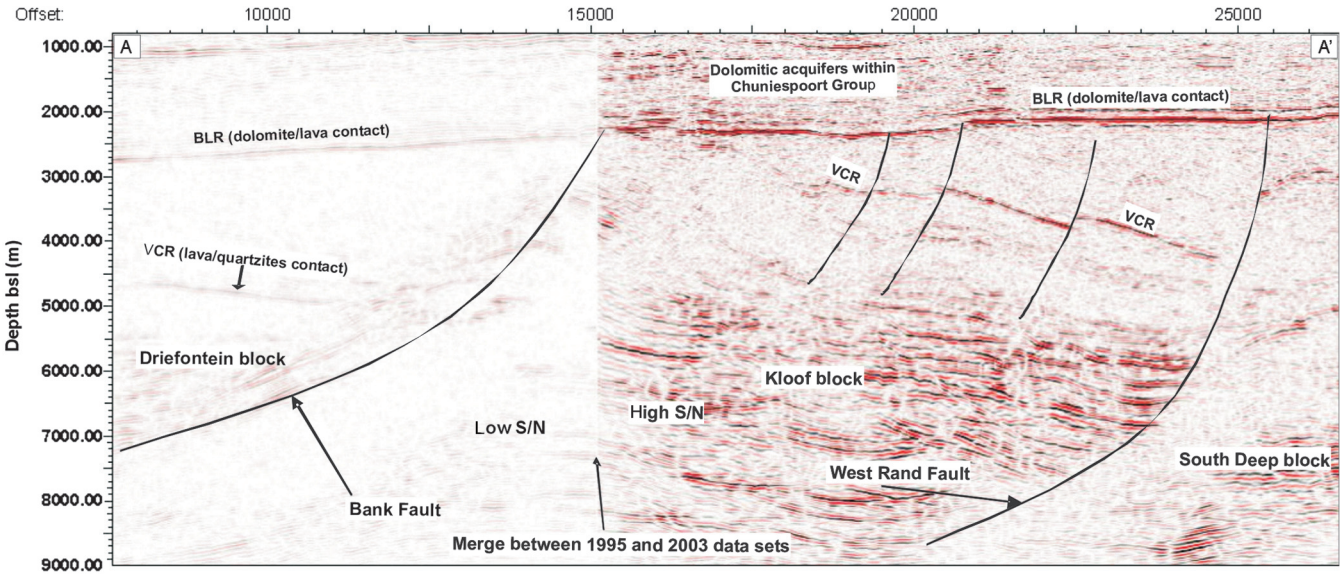


Figure 7. North–northeast regional crossline seismic section (line AA′ in Figure 6) through WUDLs, Driefontein, Kloof, and South Deep surveys. The West Rand and Bank Faults do not breach the BLR. The merge boundary between WUDLs, Driefontein, and Kloof-South Deep surveys is identifiable in the seismic section.

Figure 8. Three-dimensional visualization of the VCR edge detection attributes through Kloof and South Deep surveys. Map shows optimum imaging of structures at this horizon. The West Rand Fault (WRF) is the major structure separating Kloof and South Deep gold mines. DF: Danies Fault; DTF: Danies Twin Fault; JEF: Jocks Extension Fault; BF: Boundary Fault; S2F: Shaft 2 Fault, S4F: Shaft 4 Fault, WF: Wrench Fault, NNE 1: North-northeast 1, NNE 2: North-northeast 2.

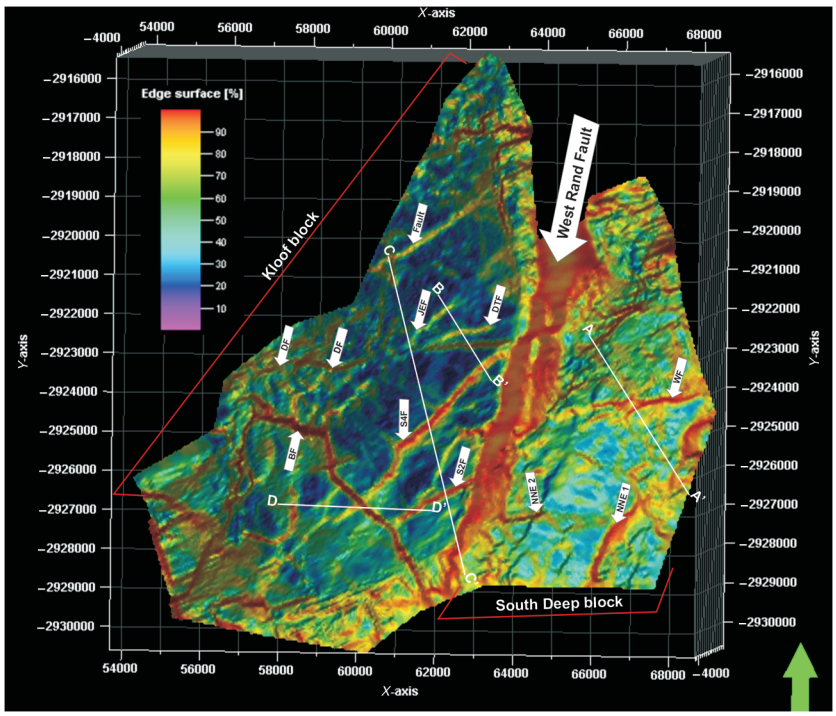

a poor migration quality, with a stretched seismic section (possibly owing to undermigration) and mis-ties between the picked horizons and borehole control (Figure 4a). The velocity field derived from boreholes was then gridded in 600-m cells, the same spacing as was used for velocity analysis. The smoothed interval velocities improved the migration quality, yielding a better tie between the picked horizons and borehole control (Figure 4b). These velocities were calibrated against the vertical seismic profile (VSP) result shown in Figure 5, which was recorded over the depth range 3100–3420 m at 5-m intervals. The purpose of the VSP was to characterize the seismic signature of stratigraphic horizons imaged by the seismic data. The borehole logging provided control for synthetic modeling and lithological discrimination.

A second pass of interactive velocity analysis was performed at 600-m intervals in crossline and inline directions and used for a migration and depth conversion (Table 2). Finally, the Kloof-South Deep and Leeudoorn PSTM data cube was merged with the WUDLs survey acquired by AngloGold Ashanti in 1995. It is important to note that the WUDLs data were never reprocessed; therefore, the data have a relatively poor signal-to-noise ratio (S/N) compared with the 2003 Kloof-South Deep data.

## INTERPRETATION AND ATTRIBUTE ANALYSIS

The topography of the reflectors marking the base of the BLR and the base of the Ventersdorp Supergroup were mapped in detail to resolve fault zones that could provide water conduits from aquifers above the BLR to VCR workings. The reflectors were prominent across the seismic volume and correlated well with synthetic seismograms computed from selected VSP data.

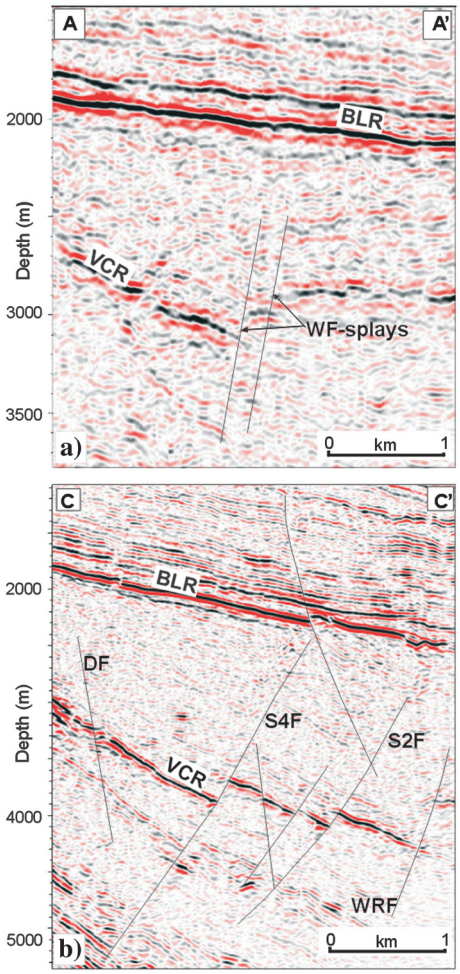


Figure 9. (a) North–northwest seismic section across the South Deep mine (line AA′ in Figure 8) showing the Wrench Fault (WF) splays. (b) North–northwest seismic section across the Kloof mine (line CC′ in Figure 8) showing the Danies Fault (DF), Shaft 4 Fault (S4F), Shaft 2 Fault (S2F) and the West Rand Fault (WRF). These faults do not crosscut the BLR on the migrated sections.

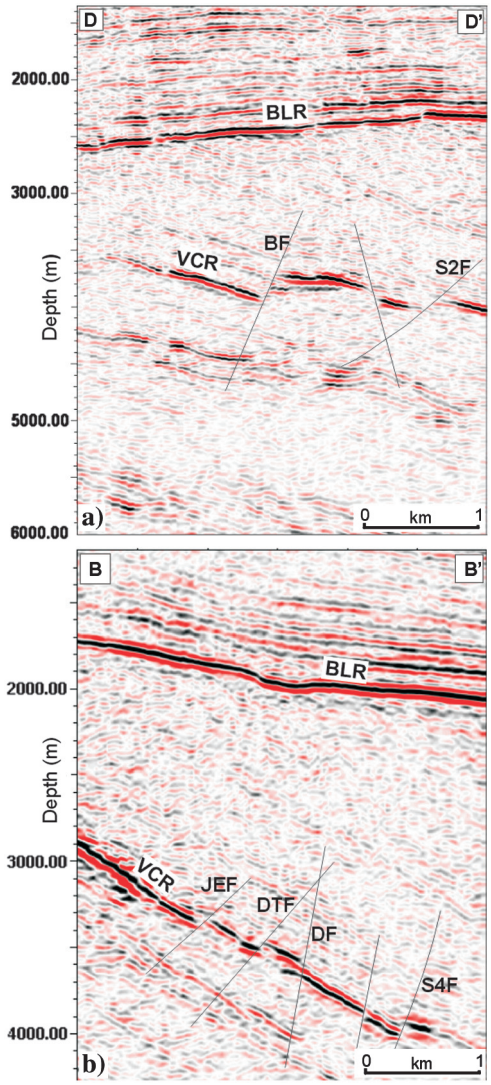


Figure 10. (a) West–east seismic section across the Kloof mine (line DD′ in Figure 8) showing a Boundary Fault (BF) and Shaft 2 Fault (S2F). (b) North–northwest seismic section (line BB′ in Figure 8) showing Jocks Extension Fault (JEF), Danies Twin Fault (DTF), Danies Fault (DF) and Shaft 4 Fault (S4F). Note that none of these faults crosscut the BLR.

The horizons and faults were manually picked on every seismic line of the depth-converted PSTM data because this was found to image faults better than auto-track picking. Even so, the smallest fault that could be manually picked on a migrated section had a throw of about one-quarter of the dominant wavelength, or about 25 m for this data set. Seismic attribute analysis was used to enhance the structural resolution further.

Attribute analysis is applied in most seismic interpretation projects where high resolution is required. We used the edge detection tools developed by Rock Deformation Research (2004) implemented in the Petrel software. The edge-detection algorithms combine dip and azimuth variations, normalized to the local noise surface, which overcomes the difference in detectability between the dip and dip azimuth attributes identified by Rijks and Jauffred (1991). Application of these edge detection techniques has contributed immensely to high-resolution imaging of structures such as faults, dikes, and fractures for the petroleum industry (Rock Deformation Research, 2004), in some cases yielding an order of magnitude increase in the number of structures imaged. The techniques also improve the lateral resolution of the fault traces, which aids in characterizing fault continuity and connectivity.

## RESULTS

### Fault mapping

The BLR and VCR reflectors are well developed throughout the area covered by the interpretation, and line-by-line manual picking provided a very robust interpretation of the VCR and BLR horizons. Numerous faults of many orientations were clearly mapped on the VCR depth structure map (Figure 6). The major West Rand and Bank Faults displace the VCR horizon by several kilometers. However, no displacement of the BLR is discernable on a seismic section (Figure 7), and thus, these faults do not appear to link aquifers in the dolomites above the BLR with the VCR stopes. However, a displacement less than the resolution limit (about 25 m) cannot be excluded. Edge detection attributes were computed for the VCR and BLR horizons to investigate possible subtle faults that appear at both elevation levels. The most prominent features revealed by edge attribute analysis of the VCR horizon in Kloof and South Deep mines, are shown on Figure 8. They include:

- West Rand Fault (WRF), a major north–northeast-trending listric fault (maximum throw ~2 km) that dips 65°–70° to the west
- Danies Fault (DF), an east-trending normal fault antithetic to the WRF that dips steeply 75°–80° to the south
- Danies Twin Fault (DTF), an east-trending normal fault synthetic antithetic to the WRF that dips steeply (76°) to the north
- Boundary Fault (BF), a north–northwest-trending normal fault antithetic to the WRF that dips steeply (70°–80°) to the southwest
- Two north–northeast-trending normal faults synthetic to the WRF, locally termed the Shaft 2 Fault (S2F) and Shaft 4 Fault (S4F), that dip moderately (50°–55°) to the west
- Wrench Fault (WF), an east-trending "dextral" strike-slip fault that separates the South Deep mine into two distinct blocks
- North–northeast-trending features synthetic to the WRF, termed NNE 1 and NNE 2, that dip 70°–80° to the west

The seismic sections in Figures 9 and 10 show structures that have displaced the VCR horizon but not the BLR. Figure 11 presents the 3D model of the VCR edge detection attribute together with the structures that are interpreted to have displaced the VCR but not the BLR. These faults were derived from the manually picked faults and remodeled to correlate with the VCR topographic breaks revealed by edge detection attributes.

The structural interpretation derived from edge detection attributes for the BLR and VCR horizons over the entire mining areas is shown in Figures 12 and 13. The edge detection attributes reveal more than 60% of structures (faults and dikes) that have propagated

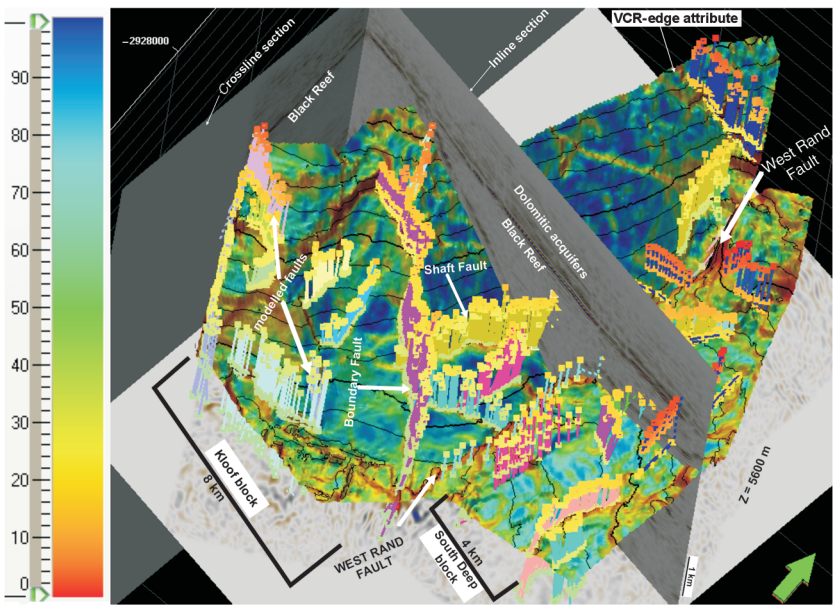


Figure 11. Three-dimensional visualization (view from southwest) of combined 3D VCR edge detection surface and modeled faults (color bar for edge detection attribute is given in%). These faults do not offset the BLR on seismic sections.

between VCR and BLR horizons (Figure 14). These include Danies Fault, Danies Twin Fault, Boundary Fault, and Shaft 4 and Shaft 2 faults in Kloof Gold Mine. In Driefontein Mine, the structures that have propagated between VCR and BLR include:

- North–northeast-trending faults adjacent to Bank Fault. These faults are situated in a structurally complex area at the down-dip edge of the survey area. The S/N is low, and thus, there is some uncertainty in their position.
- K1 and K2. The variability in their continuity on the BLR horizon could be due to variations in fault throw or oversmoothing of the BLR horizon prior to the computation of the edge attributes.
- K3, a subvertical normal fault located at the central part of the mine block. The positioning of this fault in the BLR is not precise, i.e., it is shifted slightly to the west when compared with its position in the VCR level. This mispositioning could be due to the combination of the mispicking in the seismic sections and velocity model used for migration and time-to-depth conversion.
- K4, north–northwest-trending fault in the far western part of the mine

This suggests that these faults have throws below the level required to see them on the BLR level on the seismic sections. The continuity of the several structures seen on the VCR and BLR horizons varies along the length of the structures. This could be due to variations in the throw along the fault plane. The positions and dips of Danies Fault, Boundary Fault, and Shaft Faults have been confirmed by underground mapping, whereas other seismically mapped features do not coincide with any geologically mapped structures. Importantly, most of these structures lie in areas that have not yet been mined and most of these faults have displacements below the one-quarter wavelength threshold required to pick them on a conventional seismic section. Although the area has been quite extensively drilled to map the down-dip extension of the ore bodies, the spacing between boreholes is typically greater than 1.0 km, and it is not possible to determine from borehole data alone whether differences in reef elevation of a few tens of meters between boreholes is due to faulting or folding.

Some of the faults mapped on the VCR and BLR horizons could not be tracked between the horizons on the migrated seismic sections, owing to the large vertical separation between these

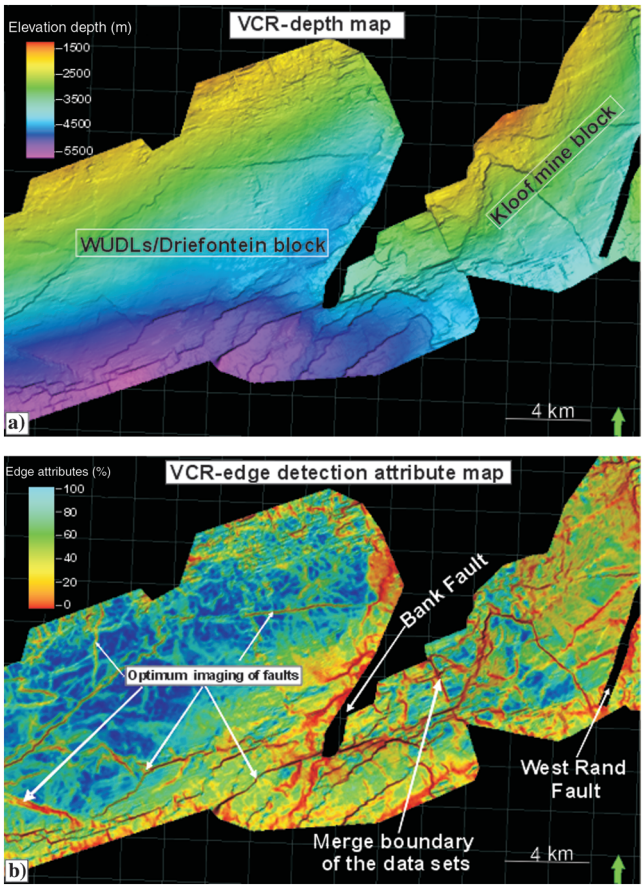


Figure 12. VCR maps showing imaging of faults before and after the computation of edge detection attributes. (a) VCR depth map (gridded) showing imaging of faults through conventional interpretation. (b) VCR edge attribute map showing high-resolution imaging of the faults, mostly with throws as small as 10 m.

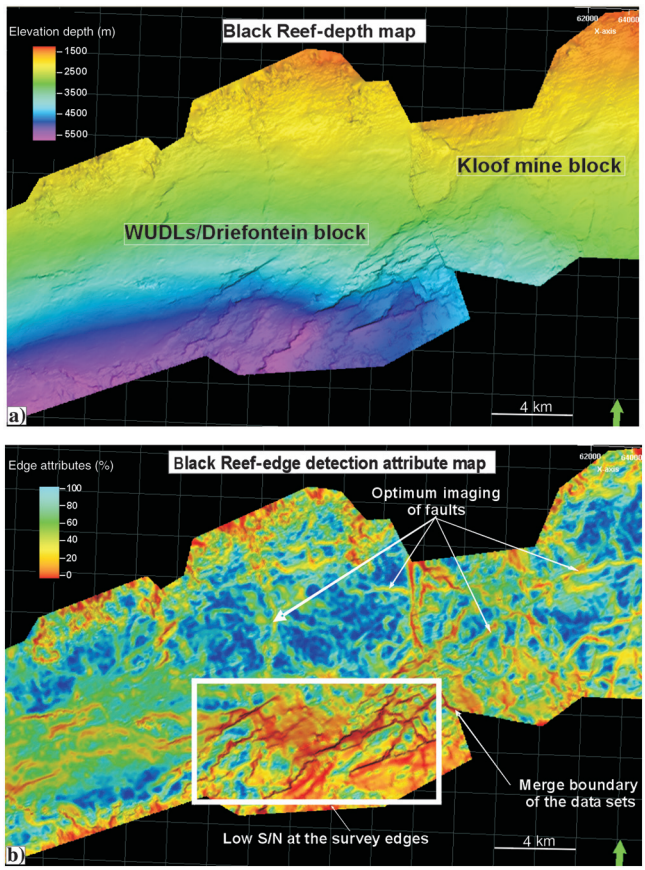


Figure 13. BLR maps showing imaging of faults before and after the computation of edge detection attributes. (a) Regional BLR depth map showing structures defined from the conventional interpretation. (b) Regional BLR edge attribute map showing high-resolution imaging of minor faults. Multicolored strips represent the subtle discrete or sharp edges on the horizon, which can be associated to low throw faults. Note the merged boundary of the data that shows up as a fault.

two horizons, poor reflectivity of markers within the Ventersdorp lavas between the two horizons, and the large range in dip angles of faults. Therefore, the linkage of displacements on the VCR and BLR levels sometimes was uncertain. However, there are many fault traces that can be confidently projected from the VCR to the BLR horizons. These may represent faults that were reactivated during the post-BLR deformation event described by Coward et al. (1995), Gibson et al. (2000), and Dankert and Hein (2010). According to D'Agostino et al. (1998) and Jackson et al. (2006), many structures in extensional basins are reactivated during later deformational events. Some structures are probably related to dikes that were emplaced after deposition of the Transvaal Basin including Bushveld, Pilanesberg, Karoo, and post-Karoo age dikes (Vermaakt and Chunnett, 1994; Coward et al., 1995; Cook, 1998; Robb and Robb, 1998).

## Relationship between faults and occurrences of fissure water and gas

A study of the relationship between the geologic structures and the occurrence of methane and groundwater was carried out at Kloof Gold Mine. The known occurrences of methane and water on the VCR horizon are shown together with the faults modeled by the Rock Deformation Research (2004) and faults interpreted from this study using edge detection attributes in Figure 15. The S/N in the northwestern portion of the Kloof survey area is low, owing to the presence of mining excavations. This reduced the confidence with which we were able to map and interpret the faults (Figure 15). Superposition of the fault map on the water and methane data suggests that structures that dip ~60° (e.g., Shaft 2 Fault and Shaft 4 Fault) or subvertically (e.g., Danies Fault) are most likely to contain water or gas.

The superposition of the VCR edge detection attribute on the water and methane data from Kloof Gold Mine shows that the Shaft 4 Fault (S4F) and Danies Fault (DF), which intersect BLR, have a good correlation with water and methane intersections (Figure 16). Water and methane often occur at several locations on a structure. The high interconnectivity and crosscutting relationship between faults (e.g., Boundary fault and Shaft 4 Fault), as shown on edge attribute maps, implies that any structure could have connectivity to aquifers above the BLR and provide a conduit for water or methane to the VCR mining horizon. These results provide high confidence that the structures that are associated with water and methane transport can be imaged by the seismic method. However, it is difficult to determine which faults and dikes intersect aquifers above the BLR and which of these aquifers may have once been charged by methane derived from coal seams. Furthermore, the ability to image the structures also is dependent on the original S/N of the manually picked horizons. A conservative approach is probably best at this stage, and to assume that any of

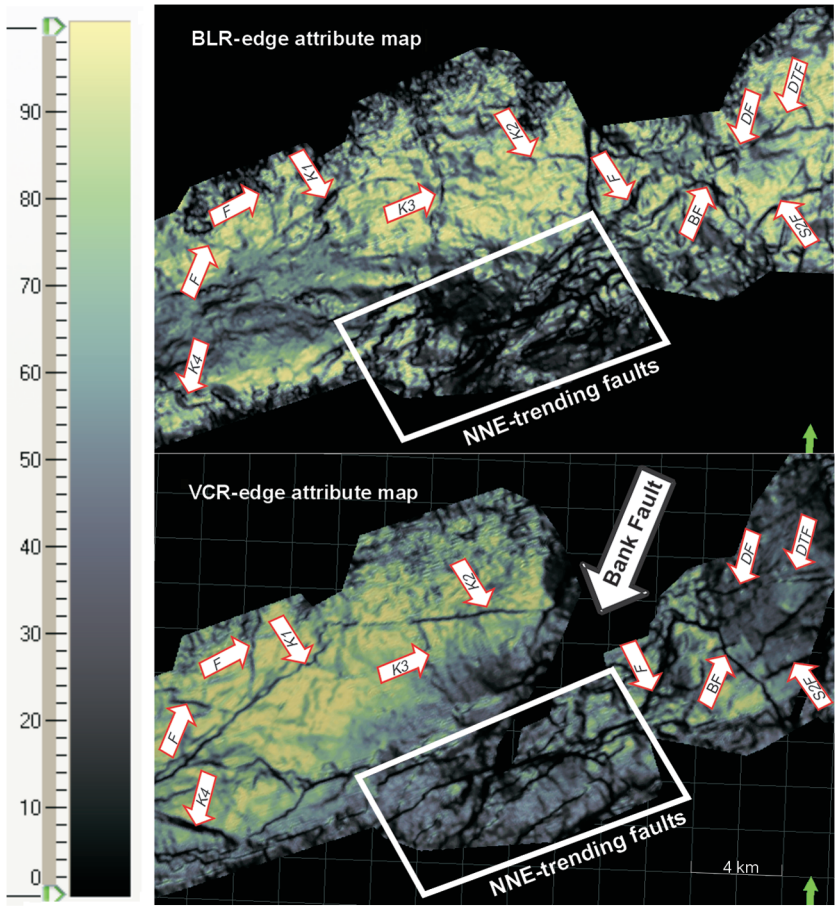


Figure 14. Propagation of faults between the BLR and VCR. BLR (top) and VCR (bottom) edge attribute maps showing high-resolution imaging of the faults. The arrows indicate structures that have propagated between the VCR and BLR horizons (color bar is given in%). DF: Danies Fault, DTF: Danies Twin Fault, BF: Boundary Fault, S2F: Shaft 2 Fault, S4F: Shaft 4 Fault, WF: Wrench Fault.

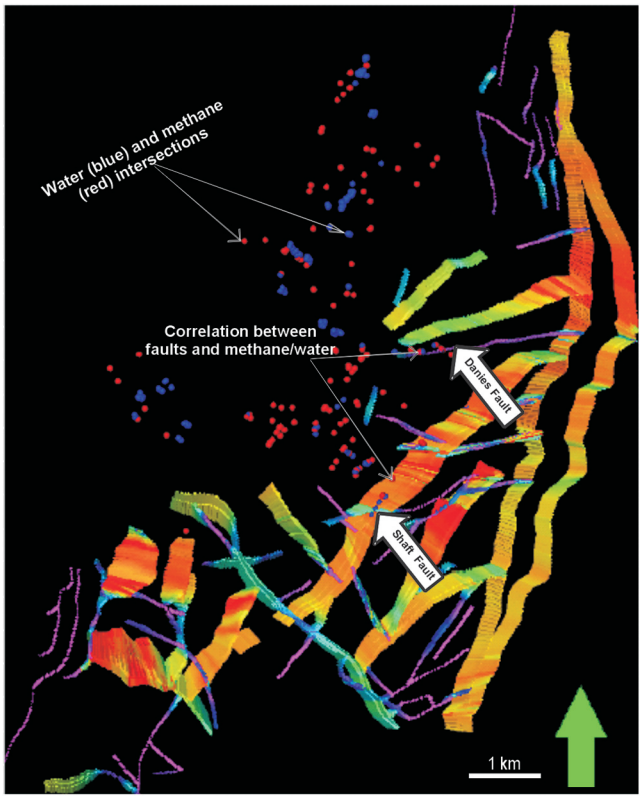


Figure 15. Seismically modeled faults and the known water-methane occurrence data in Kloof mine. There is a good correlation between methane and water, and faults, e.g., Danies Fault and Shaft Fault. Note that the northwest part of the Kloof mine has been mined out and the correlation of faults with water and methane in this area was difficult due to low S/N.

these structures could be potential conduits for water and methane. Figure 17 presents the interpreted fault surfaces, as identified by attribute analysis, differentiating between faults that are interpreted to intersect both horizons, and faults that do not intersect the BLR horizon.

## DISCUSSION

Edge detection attributes have identified a wide array of structures (fault and dikes) of different orientations and variable throws that have clearly propagated between the VCR and the BLR. These structures represent either faults that were reactivated during a post-BLR deformational event, or post-BLR intrusions. Correlation between the known occurrence of fissure water and methane with geologic- and seismic-mapped faults showed that steeply dipping structures (dip>60°) are most likely to channel fluid, although this is not a particularly useful criterion because most faults in the gold fields dip steeply. However, this study has demonstrated that water and methane occur along structures that can be mapped using 3D seismics, and thus, precautions can be taken as mining progresses. Future reports of water and methane intersections on WUDLs, Driefontein, and South Deep gold mines will be correlated with the fault model derived from edge detection attributes, and used to manage the risks associated with water and methane influx.

It is clear that large volumes of water could originate from the dolomitic aquifer overlying the BLR. However, we have not been able to identify the sources of methane with confidence. Even though the Karoo sediments and coal seams no longer overlie the West Wits Line and West Rand, it is possible that methane derived from this source entered the ground water system prior to the erosion of these strata. It also is plausible that the methane is derived from igneous intrusions or from ancient algal mats.

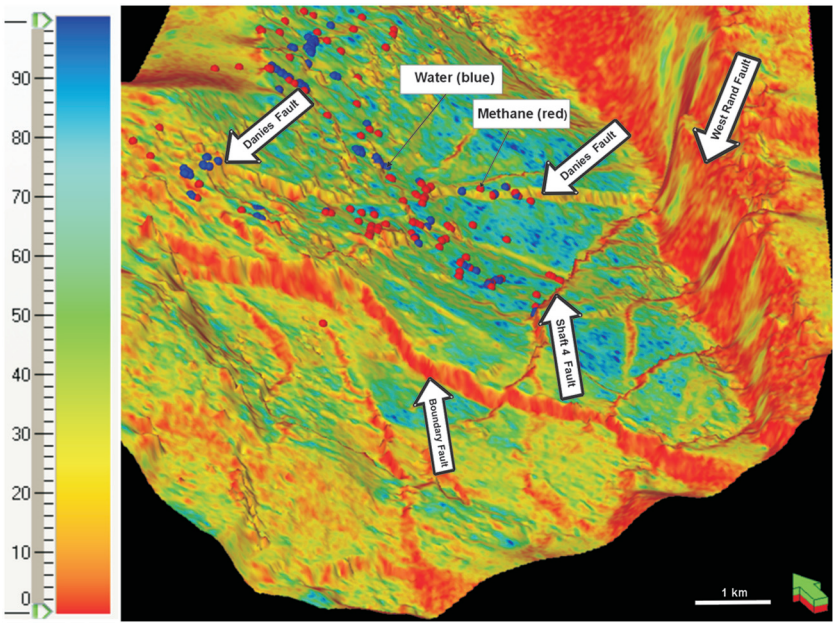


Figure 16. VCR edge attribute map of the VCR overlain with water and methane data in Kloof Mine. Structures such as Danies Fault (DF) and Shaft 4 Fault (S4F) show good correlation with water and methane data (color bar is given in %).

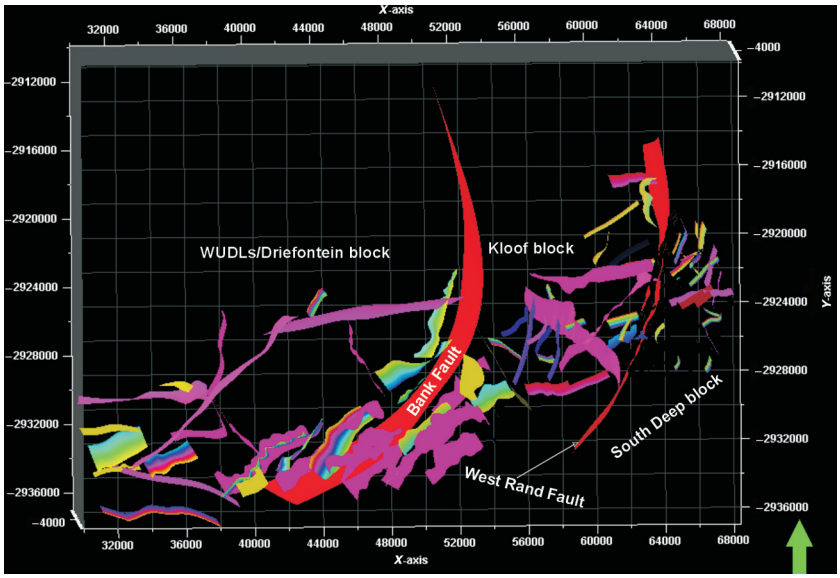


Figure 17. Fault model for WUDLs, Driefontein, Kloof, and South Deep mines using 3D seismic and edge detection attributes. The structures that have displaced the VCR and BLR are color-coded in pink.

## CONCLUSION

Reflection seismics are used widely to map ore bodies in the deep gold mines of the Witwatersrand basin. Here, we have used 3D reflection seismics to mitigate the risks to mine workers posed by water inrushes and the ignition of flammable gases. To enhance the resolution of the seismic data, horizons and faults were manually picked and edge detection attributes applied. In particular, we have identified structures that displace the VCR and BLR horizons because these are the most likely to be connected to the overlying dolomitic aquifers. We correlated the mapped occurrences of water and methane with geologic- and seismic-mapped faults, and we characterized strikes and dips of these structures and their continuity and connectivity. This information could be used to assess and mitigate the risks posed by inrushes of fissure water and the ignition of flammable gases as mining proceeds to greater depths.

## ACKNOWLEDGMENTS

This research was sponsored by Gold Fields Mining Ltd. We greatly acknowledge the thorough reviews and constructive comments of Alireza Malehmir and two anonymous reviewers, which improved the quality of the manuscript. The authors also thank Schlumberger for providing Petrel software, Rock Deformation Research Group, G. Smith, J. Trickett, L. Linzer, M. Gibson, M. Muller, S. Webb, and T. Owen-Smith for their major scientific contribution.

## REFERENCES

Adams, D., A. G. du Plessis, S. A. Gumbie, and R. P. H. Willis, 2007, Introduction to safety practices in South Africa mines: Mine Health and Safety Council Johannesburg, 210.

Beach, A., and R. Smith, 2007, Structural geometry and development of the Witwatersrand Basin, South Africa: *in* A. C. Ries, R. W. H. Butler, and R. Graham, eds., Deformation of the continental crust: The Legacy of Mike Coward, Geological Society, Special Publication, **272**, 533–542.

Bekker, E. H., 1986, Fossil water and the associated gas mixture within and below the Ventersdorp Supergroup in the Harmony mine area, Welkom goldfield: *in* C. R. Anhaeusser, and S. Maske, eds., Mineral deposits of southern Africa: Geological Society of South Africa, **1, 2**, 731–752.

Cook, A. P., 1998, The occurrence, emission, and ignition of combustible strata gases in Witwatersrand gold mines and Bushveld platinum mines, and means of ameliorating related ignition and explosion hazards: Final project report, project GAP 504, Safety in Mines Research Advisory Committee, 89.

Cousens, R. R. M., and W. S. Garrett, 1969, The flooding at the West Driefontein mine: Journal of the South African Institute of Mining and Metallurgy, **69**, 421–463.

Coward, M. P., R. M. Spencer, and C. E. Spencer, 1995, Development of the Witwatersrand Basin, South Africa, *in* M. P. Coward, and A. C. Ries, eds., Early Precambrian processes: Geological Society, Special Publication, **95**, 243–269.

D'Agostino, N., N. Chamot-Rooke, R. Funiciello, L. Jolivet, and F. Speranza, 1998, The role of pre-existing thrust faults and topography on the styles of extension in the Gran Sasso range (central Italy): Tectonophysics, **292**, 229–254, doi: 10.1016/S0040-1951(98)00070-5.

Dalley, R. M., E. C. A. Gevers, G. M. Stampfli, D. J. Davies, C. N. Gastaldi, P. A. Ruijtenberg, and G. J. O. Vermeer, 1989, Dip and azimuth displays for 3D seismic interpretation: First Break, **7**, 86–95.

Dankert, B. T., and K. A. A. Hein, 2010, Evaluating the structural character and tectonic history of the Witwatersrand Basin: Precambrian Research, **177**, 1–22, doi: 10.1016/j.precamres.2009.10.007.

Gibson, M. A. S., S. J. Jolley, and A. C. Barnicoat, 2000, Interpretation of the Western Ultra Deep Levels 3D seismic survey: The Leading Edge, **19**, 730–735, doi: 10.1190/1.1438704.

Jackson, C. A. L., R. L. Gawthorpe, and I. R. Sharp, 2006, Style and sequence of deformation during extensional fault-propagation folding: Examples from Hammam Faraun and El-Qaa fault blocks, Suez Rift, Egypt: Journal of Structural Geology, **28**, 519–535, doi: 10.1016/j.jsg.2005.11.009.

Jolley, S. J., S. R. Freeman, A. C. Barnicoat, G. M. Phillips, R. J. Knipe, A. Pather, N. P. C. Fox, D. Strydom, M. T. G. Birch, I. H. C. Henderson, and T. W. Rowland, 2004, Structural controls on Witwatersrand Gold mineralisation: Journal of Structural Geology, **26**, 1067–1086, doi: 10.1016/j.jsg.2003.11.011.

Kritzinger, P. R., 2001, Beatrix gold mine disaster. Investigation report in terms of section 64(1) of the Mine Health and Safety Act, 1996 (Act No. 29 of 1996) into the explosion which occurred on 8 May 2001: Department of Minerals and Energy (unpublished).

Malehmir, A., and G. Bellefleur, 2009, 3D seismic reflection imaging of volvanic-hosted massive sulfide deposits: Insights from re-processing of the Halfmile Lake data, New Brunswick, Canada: Geophysics, **74**, no. 6, 209–219, doi: 10.1190/1.3230495.

Malehmir, A., C. Juhlin, C. Wijns, M. Urosevic, P. Valasti, and E. Koivisto, 2012, 3D reflection seismic imaging for open-pit mine planning and deep exploration in the Kevitsa Ni-Cu-PGE deposit, northern Finland: Geophysics (this issue).

Mambane, P. W., K. A. A. Hein, S. G. Twemlow, and M. S. D. Manzi, 2011, Pseudotachylite in the South Boundary Fault at the Cooke Shaft, Witwatersrand Basin, South Africa: South African Journal of Geology, **114**, 109–120, doi: 10.2113/gssajg.114.2.109.

Manzi, M. S. D., M. A. S. Gibson, K. A. A. Hein, N. King, and R. J. Durrheim, 2012, Application of 3D seismic techniques to evaluate ore resources in the West Wits line goldfield and portions of the West Rand goldfield, South Africa: Geophysics (this issue).

McCarthy, T. S., 2006, The Witwatersrand Supergroup, *in* M. R. Johnson, C. R. Anhaeusser, and R. J. Thomas, eds., The geology of South Africa: Geological Society of South Africa, Johannesburg/Council for Geosciences, 155–186.

Milkereit, B., E. K. Berrer, A. R. King, A. H. Watts, B. Roberts, E. Adam, D. W. Eaton, J. Wu, and M. Salisbury, 2000, Development of 3-D seismic exploration technology for deep nickel-copper deposits — A case history from the Sudbury basin, Canada: Geophysics, **65**, 1890–1899, doi: 10.1190/1.1444873.

Milkereit, B., D. Eaton, J. Wu, G. Perron, M. Salisbury, E. Berrer, and G. Morrison, 1996, Seismic imaging of massive sulfide deposits, Part 2: Reflection seismic profiling: Economic Geology, **91**, 829–834, doi: 10.2113/gsecongeo.91.5.829.

Motaung, A. H. C. H., 2000, Mponeng gold mine disaster. Investigation report in terms of section 64(1) of the Mine Health and Safety Act, 1996 (Act No. 29 of 1996) into the flammable gas explosion that occurred on 29 July 1999: Department of Minerals and Energy (unpublished).

Ngcobo, T. A., 2006, The risk associated with mines in dolomite compartments: Journal of the South African Institute of Mining and Metallurgy Joernaal van die Suid-Afrikaanse Instituut vir Mynbon and Metallurgie, **106**, 251–264.

Ortlepp, W. D., 2001, The mechanism of a rock outburst in a quartzite tunnel in a deep gold mine, *in* G. Van Aswegen, R. J. Durrheim, and W. D. Ortlepp, eds., Dynamic rock mass response to mining, Proceedings of the 5th International Symposium on Rockbursts and Seismicity in Mines, South African Institute of Mining and Metallurgy Symposium Series S27, 53–58.

Pretorius, C. C., M. R. Muller, M. Larroque, and C. Wilkins, 2003, A review of 16 years of hardrock seismic of the Kaapvaal Craton, *in* D. W. Eaton, B. Milkereit, and M. H. Salisbury, eds., Hardrock seismic exploration, geophysical developments: SEG, **10**, 247–268.

Pretorius, C. C., W. H. Steenkamp, and R. G. Smith, 1994, Developments in data acquisition, processing and interpretation over ten years of deep vibroseismic surveying in South Africa: Proceedings of the 15th Congress of the Council for Mining and Metallurgical Institutions, 3, (Geology), C. R. Anhaeusser, eds., South African Institute of Mining and Metallurgy, **3**, 249–258.

Pretorius, C. C., W. F. Trewick, and C. Irons, 2000, Application of 3D-seismics to mine planning at the Vaal Reefs gold mine, number 10 shaft, Republic of South Africa: Geophysics, **65**, 1862–1870, doi: 10.1190/1.1444870.

Rijks, E. J. H., and J. C. E. M. Jauffred, 1991, Attribute extraction: An important application in any detailed 3D interpretation study: The Leading Edge, **10**, 11–19.

Robb, L. J., and V. M. Robb, 1998, Gold in the Witwatersrand Basin, *in* M. G. C. Wilson, and C. R. Anhaeusser, eds., The mineral resources of South Africa, 6th edition, Council for Geoscience, 294–349.

Rock Deformation Research, 2004, Structural and seismic appraisal of the kloof and surrounding area: Report 9350 (unpublished), 1–37.

Salisbury, M. H., G. W. Harvey, and L. Mathews, 2003, The acoustic properties of ores and host rocks in hardrock terranes, *in* D. W. Eaton, B. Milkereit, and M. H. Salisbury, eds., Hardrock seismic exploration, geophysical developments: SEG, **10**, 9–19.

Spencer, K. C., and D. M. Walter, 2000, A manual for best practice for emergency response procedures, Project Report: Turgis Technology (Pty) Ltd., 1–34.

Stevenson, F., R. M. A. Higgs, and R. J. Durrheim, 2003, Seismic imaging of precious and base-metal deposits in South Africa, *in* D. W. Eaton, B. Milkereit, and M. H. Salisbury, eds., Hardrock seismic exploration, Geophysical Development Series, SEG, **10**, 141–156.

Trickett, J. C., W. A. Duweke, and S. Kock, 2004, Three-dimensional reflection seismic: Worth its weight in platinum: International Platinum Conference 'Platinum Adding Value', South African Institute of Mining and Metallurgy, 257–264.

Vermaakt, D. T., and I. E. Chunnet, 1994, Tectono-sedimentary processes which controlled the deposition of the Ventersdorp Contact Reef within the West Wits Line, *in* C. R. Anhaeusser, ed., Proceedings of the 15th Congress of the Council for Mining and Metallurgical Institutions, **3**, (Geology): South African Institute of Mining and Metallurgy, 117–130.